Hindawi
Shock and Vibration
Volume 2024, Article ID 8891523, 14 pages
https://doi.org/10.1155/2024/8891523

Research Article

Position Optimization of Passive Patch Based on Mode Contribution Factor for Vibration Attenuation of Asymmetric 1D Structure

Dongwoo Hong,[1] Kyeongnak Lee,[2] and Byeongil Kim [3]

[1]*Daegu Mechatronics & Materials Institute, 32, Seongseogongdan-ro 11-gil, Dalseo-gu, Daegu 42714, Republic of Korea*
[2]*Neuros Co. Ltd., Daejeon-si 34027, Republic of Korea*
[3]*School of Mechanical Engineering, Yeungnam University, Gyeongsan-si 38541, Republic of Korea*

Correspondence should be addressed to Byeongil Kim; bikim@yu.ac.kr

Received 27 June 2023; Revised 24 January 2024; Accepted 13 February 2024; Published 26 February 2024

Academic Editor: Iacopo Tamellin

When the thickness of a structure is reduced to decrease weight, it may experience structural vibration and disturbance. The use of passive patches is effective in addressing this issue when the loss factor is small or when space and weight are restricted. The greatest attenuation occurs when passive patches are used across the entire coverage area. However, passive patches of reasonable size must be affixed to ensure that they are effective in terms of cost and design. In this paper, the sum of squares' value for the bending mode shape is used to determine the location of a small passive patch to achieve vibration damping for multiple modes. Under the condition of forced vibration, the modal contribution of each mode is obtained. Using this contribution as a weight, the optimal position of the passive patch is determined as the maximum value obtained in the form of a linear combination multiplied by the curvature of the beam. Simulation and experiment were used to test the efficacy of the location determined for passive patches. It was determined that, depending on the location of the passive patch, the peak amplitude at the natural frequency of each mode decreased significantly, validating the effectiveness of the design method.

1. Introduction

1.1. Research Background. In cases where resonance cannot be avoided in models with low loss factors, viscoelastic materials such as rubber are used to reduce mechanical vibration or noise. Passive patches are used when the structure to be designed has weight or space limitations. They are currently being used in a variety of fields such as the aerospace, marine, construction, and automotive fields [1]. To achieve a light weight, the thickness of the structures is reduced, and the damping effect of passive patches can be clearly observed. The passive patch also has a simple structure and is cost-effective. Additionally, research on beam structure analysis prior to patch application is being actively conducted. Baran et al. [2] investigate the influence of the Adomian decomposition method (ADM) and differential transform method (DTM) on the free vibration of Timoshenko beams and analyse the effects on variables such as axial compressive load and ground reaction force by considering boundary conditions. The results of DTM and ADM show excellent agreement, utilizing the dynamic stiffness method (DSM) to verify the mode shapes and highlighting its applicability to free vibration of beam assembly structures resting on a viscoelastic basis. Additionally, the natural frequencies and harmonic response of the cracked frame were analysed using the transfer matrix method (TMM), single variable shear deformation theory (SVSDT), and Timoshenko beam theory, and it was shown that TMM can be used for simple and efficient analysis [3–5].

The application of passive patches is divided into two categories: constrained attenuation with elastic restraint and viscoelastic layers and nonconstrained attenuation with only

viscoelastic layers. In general, the damping effect of the constrained damping technique is large. In this technique, the vibration energy dissipation due to the shear deformation of the viscoelastic layer induces attenuation [6]. The technique provides the greatest attenuation when used over the entire range. However, a passive patch of a reasonable size is more effective in terms of cost and design. Hence, the patch position is mainly determined by considering the mode with a large contribution. However, in order to achieve great efficiency using minimal passive patches, vibration analysis must be done to determine patch locations where vibration attenuation for various modes can be obtained.

Passive patches can achieve attenuation effects over a wide frequency range. Although a good attenuation effect can be obtained in the high-frequency band, the attenuation performance is insufficient in the low-frequency band. Various methods, including the Rayleigh–Ritz method, have been investigated for modeling passive patch viscoelastic materials [7, 8]. In addition, various methods have been studied for modeling viscoelastic materials used in passive patches. These include an approach for modeling passive patches for plates and beams using the Rayleigh–Ritz method to estimate the natural frequencies and loss coefficients quickly [9–13]. Modeling of harmonic excitations is proposed when a passive patch and an active patch are installed [14]. In such a case, it is necessary to optimize the position of a small passive patch before applying the active patch. In the case of passive patches, the result is affected not only by the position of the patch's bending shape function but also by the loss factor of the viscoelastic layer, the shear coefficient, thickness, length, elastic modulus and thickness of the lower object to be controlled, and the length of the passive patch [13]. Thus, the effects of the previous parameters on the design of passive patches have been studied [13, 15, 16].

To optimize the position of a passive patch, Zheng et al. minimized the length and position of the patch by using a genetic algorithm based on the penalty function method [17, 18]. Lei and Zheng have optimized the passive patch location through topological optimization of the penalization model [19, 20], and Fang has used the level set method [21]. Araujo et al. performed optimization using the Feasible Arc Interior Point Algorithm (FAIPA) to derive the maximum loss factor [22]. El Hafidi et al. optimized patch location and improved algorithm convergence through genetic algorithms and Latin Hypercube Sampling (LHS) algorithms [23]. Askar et al. used a genetic algorithm to optimize the position of the circular aluminium patch [24]. The literature review indicates that various algorithms have been used to optimize the position of the passive patch. However, a simple and quick design method is required to determine the optimal position of a passive patch in real industrial fields.

1.2. Objectives. In this paper, a method to optimize the position of a passive patch with a certain length and thickness is introduced to 1D structures, especially for use with cantilevered beams. First, the method of obtaining the frequency response, natural frequency, and mode loss coefficient is described, which is based on the analytical model for beams with passive patches expressed by complex stiffness. Next, the change in the natural frequency and the loss factor for each mode of the passive patch of a certain length are examined.

Although the position of the passive patch can be determined using the above method, it would be simpler to use the beam shape function. Considering the wide frequency range, the sum of squares using the bending shape function of the beam is obtained together with the modal contribution by the specific excitation range. Subsequently, the position of the appropriate patch is determined and then verified through experiments using the predicted results.

This paper is organized as follows. Section 2 describes the approximate model of the existing passive patch, and Section 3 analyses and explains the characteristics of the passive patch through simulation. Then, the optimal position of the passive patch is determined by using the sum of squares of the proposed bending shape function, and the performance of the designed passive patch is analysed. Finally, Section 4 discusses conclusions and future plans.

2. Modeling

2.1. Beam with a Patch. A cantilever beam model with a passive patch is shown in Figure 1.

In a thin Euler beam of fixed length L, a passive patch of short beam shape with length L_x consisting of a viscoelastic layer and a confining layer is attached at position x_p. Disturbance acts in the form of harmonic function at position x_d, which has 5 cm from fixed point, where the length L of the beam is assumed to be sufficiently longer than the width L_y of the beam. As the beam is thin, the deformation in the thickness direction is neglected and the material of the beam is assumed to be isotropic, homogeneous, and linear elastic with the same properties in all directions.

Here, the lower beam is defined as layer 3, the viscoelastic layer as layer 2, and the constraint layer as layer 1. Figure 2 shows the deformation due to bending of each layer. The subscript denotes the layer number, w is the transverse displacement, u is the longitudinal displacement, ψ is the rotation angle, and γ is the shear angle.

2.2. Displacement Vector. The motion of each layer was investigated by Kung and Singh [5, 6]. The displacement vector $\mathbf{r}$ representing the motion of each layer is defined as the following equation (1). The superscript p represents the number of the layers.

$$\mathbf{r}_1^p = \begin{Bmatrix} w \\ u_1^p \\ \psi_1^p \end{Bmatrix}, \mathbf{r}_2^p = \begin{Bmatrix} w \\ u_2^p \\ \psi_2^p \end{Bmatrix}, \mathbf{r}_3 = \begin{Bmatrix} w \\ u_3 \\ \psi_3 \end{Bmatrix}. \quad (1)$$

The displacement vector $\mathbf{r}$ is assumed to be temporally and spatially continuous. It is assumed that the lateral displacement w in layers 1 and 2 is equal to the displacement

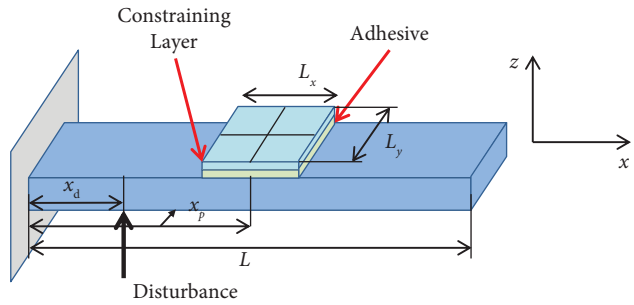

Figure 1: Cantilever beam with passive patch.

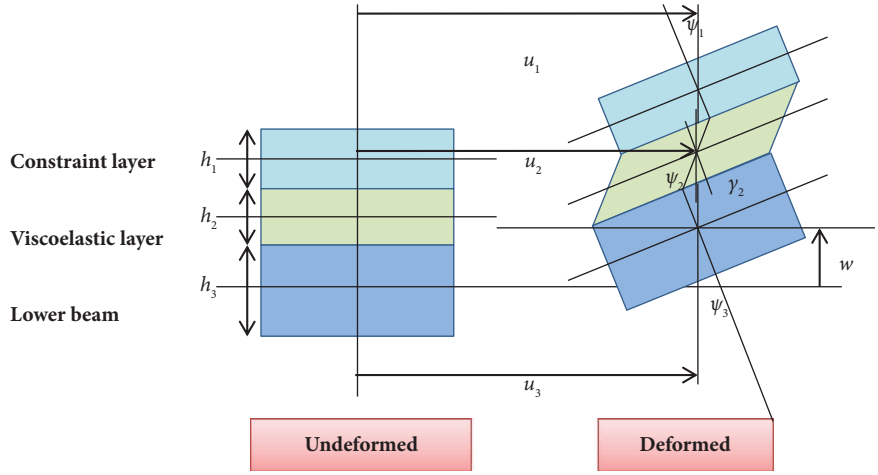

Figure 2: Before and after deformation of passive patch structure.

w in the lower layer. As the shear rate of layers 1 and 3 is larger than that of layer 2 ($G_2^p \ll G_1^p, G_3^p$), the shear angle is assumed to be negligible ($\gamma_1, \gamma_3 \ll \gamma_2$) as shown in Figure 2, which is much smaller than the viscoelastic layer. Therefore, the total angle of rotation at layers 1 and 3 is equal to the partial differential of the bend ($\psi_1 = \psi_3 = \partial w/\partial x$). The rotation angle in layer 2 is defined as $\psi_2 = \partial w/\partial x - \gamma_2$, which is the difference between the partial derivative of the bend and the shear angle.

Let us assume that the bending displacement w in the orthogonal coordinate z direction at an arbitrary position $x$on the vibrating beam can be expressed by the sum of the terms multiplied by the shape function $\phi_{w,k}(x)$ of the k-th mode and the weighting function $q_k(t)$ as follows. The continuous system has infinite degrees of freedom, but this problem has N degrees of freedom if it is sufficient to consider it as a linear combination of the product of the N shape functions and the weighting factors. At this time, the lateral displacement w is expressed by the following equation (2):

$$w(x,t) = \phi_{w,1}(x)q_1(t) + \phi_{w,2}(x)q_2(t) + \cdots + \phi_{w,N}(x)q_N(t) = \sum_{k=1}^{N} \phi_{w,k}(x)q_k(t) = \mathbf{\Phi}_w \mathbf{q}(t) = \mathbf{\Phi}_w \mathbf{q} e^{j\omega t}. \tag{2}$$

Here, q_k is a weighting function for each mode. Both the disturbance and the response are assumed to be a harmonic function of a certain size. Φ_w is a shape function vector of size $1 \times N$ and $\mathbf{q}$ is a weight vector of size $N \times 1$. Through these two functions, the shape function S can be organized as follows:

$$\mathbf{\Phi}_w(x) = \{\phi_{w,1}(x), \ldots \phi_{w,k}(x) \ldots \phi_{w,N}(x)\},$$
$$\mathbf{q}(t) = \{q_1(t), q_2(t), \ldots, q_k(t), \ldots, q_N(t)\}^T, \tag{3}$$
$$\mathbf{S} = \left[\mathbf{\Phi}_w \mathbf{\Phi}_u \mathbf{\Phi}_\psi\right]^T = [\mathbf{S}_1 \cdots \mathbf{S}_k \cdots \mathbf{S}_N].$$

2.3. Mass Matrix and Stiffness Matrix. In the case of inertia matrix H, it is a matrix derived in the process of defining the mass matrix. First of all, kinetic energy is defined by shape function and weight as follows:

$$T = \frac{1}{2}\sum_{k=1}^{N}\sum_{j=1}^{N} q_k q_j \int \phi_{w,k}(x)\phi_{w,j}(x)dm = \frac{1}{2}\sum_{k=1}^{N}\sum_{j=1}^{N} m_{kj} q_k q_j. \tag{4}$$

In this equation, the generalized mass is $m_{kj} = \int \phi_{w,k}(x,y)\phi_{w,j}(x,y)dm$ and the integration is performed over the bin length. If it is a plate of ρ with a thickness of h in a continuous system made up of infinitesimal masses, it can be expressed as $dm = \rho bh dx$. For the rotational displacement $\psi(x,t)$, the infinitesimal mass is $dm = \rho(bh^3/12)dx$ and the generalized mass using integration can be expressed as follows:

$$m_{w,kj} = \int \phi_{w,k}(x)\phi_{w,j}(x)\rho bh dx,$$
$$m_{\psi,kj} = \int \phi_{\psi,k}(x)\phi_{\psi,j}(x)\rho b\left(\frac{h^3}{12}\right)dx. \quad (5)$$

Using the shape function vector, the mass matrix can be expressed as shown, and the inertia matrix H is defined based on this equation:

$$\mathbf{M}_w = \int \mathbf{\Phi}_w^T(x)\mathbf{\Phi}_w(x)\rho bh dx, \quad (6)$$

$$\mathbf{M}_u = \int \mathbf{\Phi}_u^T(x)\mathbf{\Phi}_u(x)\rho bh dx, \quad (7)$$

$$\mathbf{M}_\psi = \int \mathbf{\Phi}_\psi^T(x)\mathbf{\Phi}_\psi(x)\rho\left(\frac{bh^3}{12}\right)dx. \quad (8)$$

The mass matrix $\mathbf{M}$ of size $n \times n$ is in the form of a superposed mass matrix using the inertia matrix $\mathbf{H}$ and the shape function matrix $\mathbf{S}$ of size $3 \times N$.

$$\mathbf{M} = \int \mathbf{S}^T\mathbf{H}\mathbf{S}dx. \quad (9)$$

Here, the inertia matrix $\mathbf{H}$ is expressed by equation (10).

$$\mathbf{H} = \rho b\begin{bmatrix} h & 0 & 0 \\ 0 & h & 0 \\ 0 & 0 & \dfrac{(h)^3}{12} \end{bmatrix}. \quad (10)$$

Thus, the kinetic energy of equation (11) is finally expressed as follows. The relationship between the displacement vector $\mathbf{r}$ and the generalized displacement vector $\mathbf{q}$ can be expressed with the matrix of shape functions $\mathbf{S}(x)$ [9].

$$T = \frac{1}{2}\int \dot{\mathbf{r}}^T\mathbf{H}\dot{\mathbf{r}}dx = \frac{1}{2}\dot{\mathbf{q}}^T(t)\int\int_A \mathbf{S}^T(x)\mathbf{H}\mathbf{S}(x)dx\dot{\mathbf{q}}(t) = \frac{1}{2}\dot{\mathbf{q}}^T(t)\mathbf{M}\dot{\mathbf{q}}(t). \quad (11)$$

In the case of strain energy (potential energy), the displacement is restored by the deformation in the vibrating beam and converted into motion. In the case of a linear elastic body, the energy is expressed as the product of the force and the strain, such that $U_i = (1/2)F_iu_i$. The value $U = \sum_{i=1}^n U_i = (1/2)F_iu_i$ added by the energy density to the entire beam becomes the total strain energy of the beam. The integral of each energy density equation is integrated over the length, and the displacement vector $\mathbf{r}$ is summarized as follows:

$$U = \int_L \frac{1}{2}\left(\mathscr{D}\begin{bmatrix} w \\ u \\ \psi \end{bmatrix}\right)^T \mathbf{E}\left(\mathscr{D}\begin{bmatrix} w \\ u \\ \psi \end{bmatrix}\right)dx = \int_L \frac{1}{2}(\mathscr{D}\mathbf{r})^T\mathbf{E}(\mathscr{D}\mathbf{r})dx. \quad (12)$$

Here, the differential operator $\mathscr{D}$ and the elasticity matrix $\mathbf{E}$ are as follows [9]:

$$\mathscr{D} = \begin{bmatrix} \dfrac{\partial^2}{\partial x^2} & 0 & 0 \\ \dfrac{\partial}{\partial x} & -1 & 0 \\ 0 & 0 & \dfrac{\partial}{\partial x} \end{bmatrix}, \mathrm{E} = \begin{bmatrix} D_E & 0 & 0 \\ 0 & EA & 0 \\ 0 & 0 & GA \end{bmatrix}. \quad (13)$$

Equation (6) is summarized as follows through equation (2):

$$U = \int_L \frac{1}{2}(\mathscr{D}\mathbf{r})^T\mathbf{E}(\mathscr{D}\mathbf{r})dx = \int_L \frac{1}{2}(\mathscr{D}\mathbf{S}(x)\mathbf{q}(t))^T\mathbf{E}(\mathscr{D}\mathbf{S}(x)\mathbf{q}(t))dx$$
$$= \frac{1}{2}\mathbf{q}^T(t)\int_L (\mathscr{D}\mathbf{S}(x))^T\mathbf{E}(\mathscr{D}\mathbf{S}(x))dx\,\mathbf{q}(t) = \frac{1}{2}\mathbf{q}^T(t)\mathbf{K}\mathbf{q}(t). \quad (14)$$

Here, the stiffness matrix $\mathbf{K}$ is as follows:

$$\mathbf{K} = \int_L (\mathscr{D}\mathbf{S}(x))^T\mathbf{E}(\mathscr{D}\mathbf{S}(x))dx. \quad (15)$$

For each layer, both the mass matrix and the inertia matrix are added to obtain the kinetic energy and strain energy of the whole, and the integral range corresponds to the length of each layer. The mass matrix M and the stiffness matrix K for the entire layer are defined as follows:

$$\mathbf{M} = \sum_{p=1}^{N_p}\int_{L_p}\left[\mathbf{S}_1^{\mathrm{pT}}\mathbf{H}_1^p\mathbf{S}_1^p + \mathbf{S}_2^{\mathrm{pT}}\mathbf{H}_2^p\mathbf{S}_2^p\right]dx + \int_L \mathbf{S}_3^T\mathbf{H}_3\mathbf{S}_3dx, \quad (16)$$

$$\mathbf{K} = \sum_{p=1}^{N_p}\int_{L_p}\left[\left(\mathscr{D}\mathbf{S}_1^p\right)^T\mathbf{E}_1^p\left(\mathscr{D}\mathbf{S}_1^p\right) + \left(\mathscr{D}\mathbf{S}_2^p\right)^T\mathbf{E}_2^q\left(\mathscr{D}\mathbf{S}_2^p\right)\right]dx + \int_L (\mathscr{D}\mathbf{S}_3)^T\mathbf{E}_3(\mathscr{D}\mathbf{S}_3)dx. \quad (17)$$

By substituting equation (17) into equations (11) and (14), the kinetic energy and strain energy for the whole system are calculated.

2.4. Approximation. When an object is assumed to have N vibration modes, its degree of freedom is N. Since the beam with several passive patches has a multiple number of subparts including base layer, adhesives, and patches, the total degree of freedom would be increased by the multiple of part numbers. Therefore, to simplify the problem, it is necessary to reduce the degree of freedom for calculation. Here, it is assumed that the motion of the passive patch is determined with respect to the bending shape function of the base layer. First, in the case of the base layer, the Euler beam is fixed on one side. For the beam, the eigenvalue can be analytically calculated through the characteristic equation and then the normalized shape function can be obtained.

$$\phi_{w,k} = \frac{1}{\sqrt{\int_0^{L_x}\left(\phi_{w,k}\right)^2 dx}}\left[\cos h\beta_k x - \cos\beta_k x - \frac{\sin h\beta_k l - \sin\beta_k l}{\cos h\beta_k l + \cos\beta_k l}\left(\sin h\beta_k x - \sin\beta_k x\right)\right], \tag{18}$$

$$\cos h\left(\beta_k L\right)\cos\left(\beta_k L\right) = -1, \quad k = 1, 2, 3, \cdots.$$

For the remaining shape functions, the Rayleigh–Ritz method using strain energy can be expressed as a linear combination of the permissible function satisfying the boundary condition, or the natural frequency can be approximated without solving the complex eigenvalue problem through the weak-core hypothesis.

First, the relationship of motion between layers is considered a weak-core assumption, [21] is applied as the modulus of elasticity of the middle viscoelastic layer, it is smaller than that of the beam, and the constraint layer in the structure of the laminated layer in which the axial load is applied. The longitudinal displacement of layer 1 and layer 3 has the following relationship:

$$\frac{E_1^p h_1^p}{1-\left(\nu_1^p\right)^2}\frac{\partial u_1^p}{\partial x} + \frac{E_3 h_3}{1-\left(\nu_3\right)^2}\frac{\partial u_3}{\partial x} = 0$$

$$\Rightarrow \frac{\partial \phi_{u,1}^p}{\partial x} + e^p\frac{\partial \phi_{u,3}}{\partial x} = 0, e^p = \frac{E_3 h_3\left[1-\left(\nu_1^p\right)^2\right]}{E_1^p h_1^p\left[1-\left(\nu_3\right)^2\right]}, \quad p = 1, \ldots, N_p. \tag{19}$$

Integrating equation (19) with x yields the following:

$$\phi_{u1,k} = -e^p\phi_{u3,k} + d_k^p, \tag{20}$$

where d_k^p is a constant for indicating the relationship of the shape function. Next, the longitudinal displacement u_1, u_3 and the rotational angle ψ_1, ψ_3 in layer 2 can be expressed using the longitudinal displacement u_2 and the rotational angle ψ_2 of layers 1 and 3. The relationship is represented in Figure 3. For each passive patch, the shape function for each mode can be expressed as equations (21) and (22):

$$\phi_{u2,k} = \frac{1}{2}\left[\left(\phi_{u3,k} - \frac{h_3}{2}\phi_{\psi 3,k}\right) + \left(\phi_{u1,k} + \frac{h_1}{2}\phi_{\psi 1,k}\right)\right], \tag{21}$$

$$\phi_{\psi 2,k} = \left(\frac{1}{h_2^q}\right)\left[\left(\phi_{u3,k} - \frac{h_3}{2}\phi_{\psi xz3,k}\right) - \left(\phi_{u1,k} + \frac{h_1}{2}\phi_{\psi 1,k}\right)\right]. \tag{22}$$

2.5. Natural Frequency and Loss Factor. The natural frequency and mode loss factor for each mode can be obtained from the strain energy and kinetic energy obtained previously. First, the loss factor is expressed as complex stiffness in the stiffness matrix. The complex modulus of elasticity is expressed as $E^* = E(1 + j\eta)$. Here, $*$ denotes a complex value. In the case of the viscoelastic layer, the shear factor and the loss factor η depend on the frequency. Therefore, the modulus of elasticity is expressed as $E_2^*(\omega)$. The total strain energy and kinetic energy written in complex stiffness are as follows:

$$U^* = \frac{1}{2}\mathbf{q}^T(t)\mathbf{K}^*(\omega)\mathbf{q}(t), T = \frac{1}{2}\dot{\mathbf{q}}^T(t)\mathbf{M}\dot{\mathbf{q}}(t). \tag{23}$$

At this time, as the response is assumed to be a harmonic response, the complex eigenvalue problem in free oscillation can be written as follows:

$$\left[\mathbf{K}^*(\omega) - \omega^2\mathbf{M}\right]\mathbf{q} = \mathbf{0}, \lambda_k^* = \mathbf{M}^{-1}\mathbf{K}^*. \tag{24}$$

In this case, as the stiffness matrix has a frequency dependent characteristic, the eigenvalue converges through iterative calculation. In equation (24), λ_k^* represents the complex eigenvalue. The natural frequency and loss coefficient can be defined from the complex eigenvalue λ_k^*.

2.6. Forced Vibration by Disturbance. When the disturbance is applied to a point of the beam, it is assumed that only the bending is generated and the disturbance vector $\mathbf{Q}$ is defined as follows:

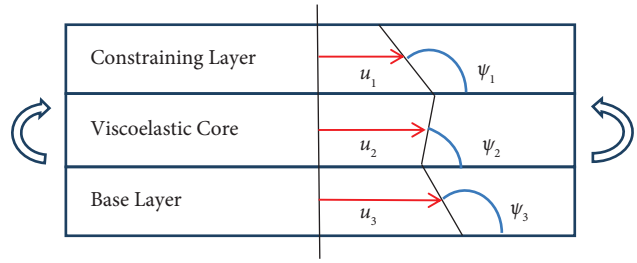

Figure 3: Motion relationship of each layer.

$$\mathbf{Q} = \int_L F(x)\mathbf{\Phi}_w(x)dx, \tag{25}$$

where F represents the magnitude of the disturbance for each mode. This is nonconservative and is added to the right side of the equation of motion in equation (24). At this point, by calculating the weight vector $\mathbf{q}$, the displacement of the beam can be calculated, and the displacement of the remaining layers is also determined.

$$\mathbf{q} = \left[\mathbf{K}^*(\omega) - \omega^2\mathbf{M}\right]^{-1}\mathbf{Q}. \tag{26}$$

When disturbance in the form of harmonic function acts on a point x_d, $F(x,t)$ is expressed as follows:

$$F(x,t) = F\delta(x - x_d)e^{j(\omega t+\theta)}. \tag{27}$$

Then, the disturbance vector $\mathbf{Q}$ is calculated, and equation (26) is summarized as follows:

$$\mathbf{q} = \left[\mathbf{K}^*(\omega) - \omega^2\mathbf{M}\right]^{-1}F\mathbf{\Phi}_w(x_d)e^{j\theta}. \tag{28}$$

Here, the Fourier transform can be taken to calculate the frequency response.

$$H(\omega) = \int_{-\infty}^{\infty}\mathbf{q}(t)e^{-j\omega t}dt = \left[\mathbf{K}^*(\omega) - \omega^2\mathbf{M}\right]^{-1}F\mathbf{\Phi}_w(x_d)e^{j\theta}. \tag{29}$$

3. Simulation and Experiment

3.1. Loss Coefficient Variation. First, simulation was performed on the length of a passive patch in order to check how the loss of each mode changes depending on the position of the passive patch. The material, properties, and shape of the lower beam and passive patches were determined as shown in Table 1, with reference to the viscoelastic layer used in Plattenburg et al. [12].

The natural frequencies calculated for beams without passive patches are given in Table 2. The first target is the vibration attenuation for the five modes of the beam, with the patch designed to attenuate vibrations of 0–1000 [Hz]. The length L of the beam will be normalized, and other parameters will be expressed for the length of the beam. The normalized mode shape of the lateral vibration of the cantilever beam is shown in Figure 4. As the shape function does not change even when the patch is attached, the design of the patch depends on the mode shape [25].

When the mode shape of the beam is viewed, the shortest distance between nodes is mode 5 and the distance corresponds to a normalized length of 0.2. Therefore, the normalized length corresponding to 1/2 of the distance between nodes is determined as 0.1.

This condition enables the simulation of the manner in which the loss factor for each mode is affected by the position of the patch. The position of the patch has a finite length, so it shows when the position changes from 0.01 to 0.95 from the normalization position of 0.05. Figure 5 shows the second derivative of the mode shapes. For each mode, the correlation between the magnitude of the second-order differential absolute value $|\partial^2 w/\partial x^2|$ of the normalized bend shape and the loss factor can be observed by plotting these on the graph simultaneously.

In Figure 6, the loss factor for the 1st and 2nd modes and the curvature of the beam are shown for example. Similar trends have been observed for 3rd, 4th, and 5th modes as well. It is confirmed that the magnitude of the absolute value of the second derivative w'' of the mode shape is proportional to the magnitude of the second derivative w''. The second-order derivative w'' of the mode shape is the curvature κ of the beam, and the larger the size, the more effective the attenuation of the passive patch. The reason is that the larger the curvature κ of the beam, the greater the magnitude of the moment acting on the beam. Further, the strain on the beam surface increases and affects the motion of the patch. When the curvature κ is seen, the fixed part of the beam has the largest value. However, as it is difficult to attach a patch having a finite length to the fixed portion, it is excluded from the attachment position of the passive patch.

Figures 7 and 8 show the variation of the natural frequency according to the position of the passive patch. Additionally, Table 3 summarizes the natural frequency changes according to the patch location. It is observed that the value of the natural frequency changes greatly as the degree of the mode increases. In addition, when the passive patch is installed near the fixed end, the natural frequency is observed to be high in all modes, whereas when it is attached near the free end, it is confirmed that the natural frequency is lowered.

3.2. Optimal Patch Location. The influence of the curvature of the beam was confirmed. Thus, the values for the curvature of the beam are utilized to design the patch. The position x_d in the beam does not change the mode shape.

Table 1: The physical properties and shape of each layer.

	Constrained	Viscoelastic layer	Beam	Unit
Material	Aluminium	Adhesive	Steel	
Modulus of elasticity	69×10^3	$6.2 + 2.2 \times 10^{-2} f$ [Hz]	190×10^3	MPa
Density	2730	730	7870	kg/m^3
Poisson Ratio	0.33	0.4	0.3	
Loss factor	0.005	$1.25 - 3.7 \times 10^{-4} f$ [Hz]	0.0013	
Thickness	0.8	1.14	3	mm
Length	40	40	400	mm

Table 2: Natural frequency of beam.

Unit: (Hz)	Mode 1	Mode 2	Mode 3	Mode 4	Mode 5
Natural frequency	14.9	93.3	261.2	511.7	845.9

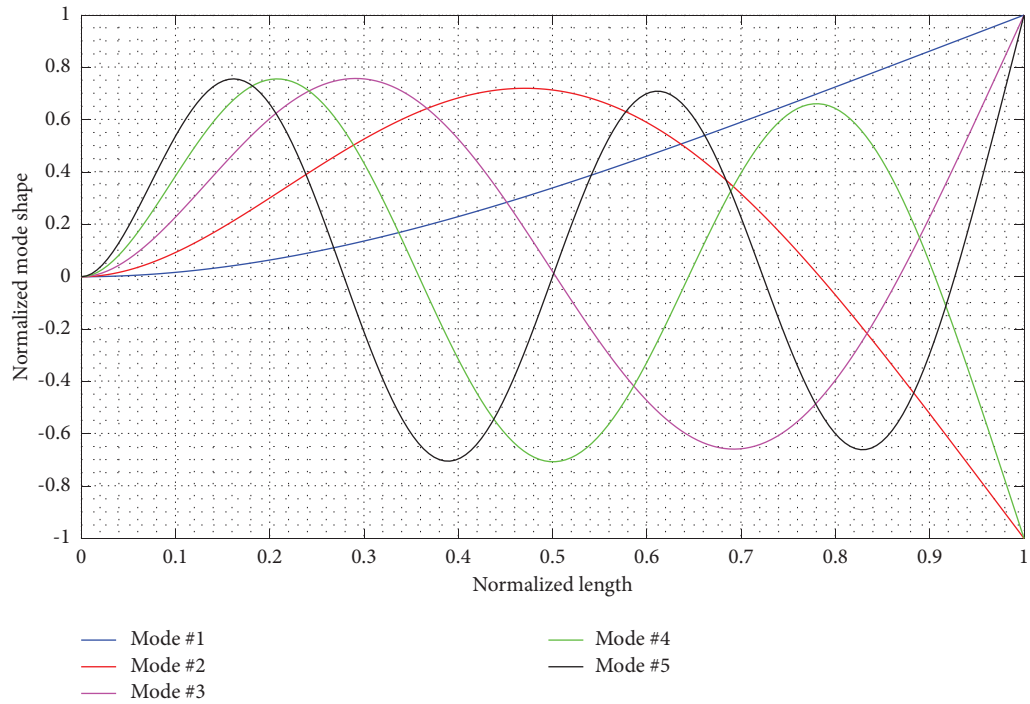

Figure 4: Five mode shapes of beam.

However, the contribution of each mode changes. As the mode contribution Γ_k of each mode represents the degree of contribution of the mode and the attenuation across the beam is aimed at all the frequency bands, the mode contribution is determined only by the exciter, and unlike the weight vector **q** defined above, it is defined as in equation (30). If a frequency band is mainly used, the mode contribution should be estimated considering only the modes within the frequency band.

$$\Gamma_k = \frac{\int_L F(x)\phi_{w,k}(x)dx}{\sum_{k=1}^{N}\int_L F(x)\phi_{w,k}(x)dx}. \tag{30}$$

If the value of the excitation magnitude $F(x)$ is a constant probability in the range of 0.05 to 0.1, the modal contribution for each mode is calculated as given in Table 4.

For mode contribution, mode 4 and mode 5 are large. Each mode contribution is weighted and multiplied by the second derivative $\phi''_{w,k}$ of the mode shape to be squared and then added. Ss denotes the sum of squares.

$$w''_{ss}(x, f) = \sum_{k=1}^{N}\left(\phi''_{w,k}(x)\Gamma_k\right)^2. \tag{31}$$

Using the mode contributions calculated in Table 4 and the values in Figure 5, the sum of squares of the shape functions can be plotted as shown in Figure 9. In this case, the position of the passive patch can be selected as 0.19, 0.41, 0.59, 0.82 except for the normalized positions 0 and 1 given the length of the patch is finite. However, as the size is largest at 0.82, the optimum patch position is determined to be 0.82. In order to compare the effect of the patch position, two cases of passive patches with the normalized length of 0.82

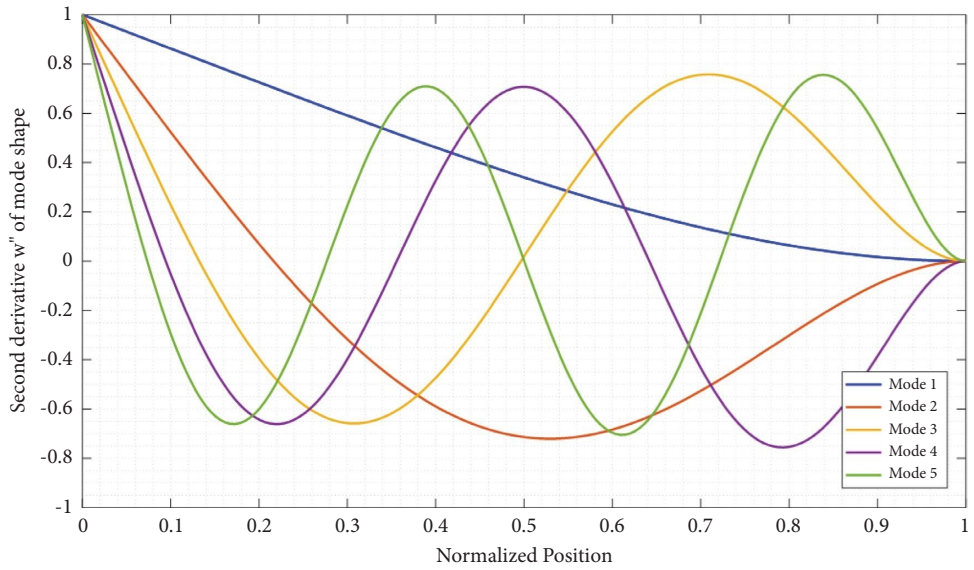

Figure 5: The second derivative of the beam's five mode shapes.

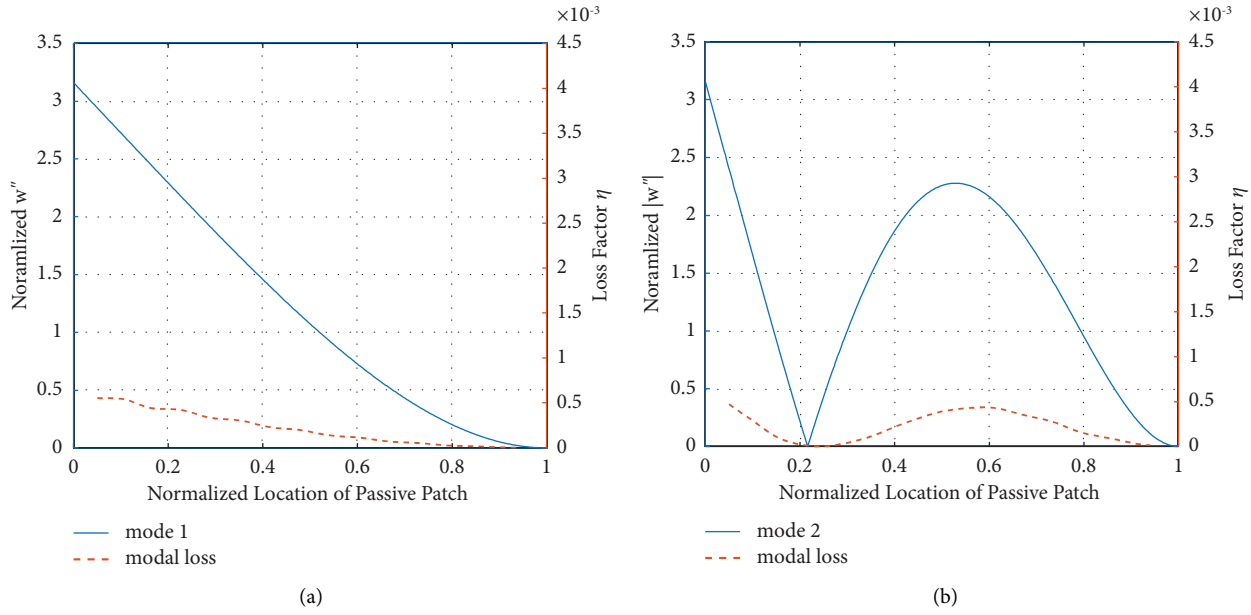

Figure 6: The loss factor for the (a) 1st mode and (b) 2nd mode and the curvature of the beam.

and the low value of 0.5 are compared to predict the performance of the passive patch by simulation. In this case, 0.5 is selected because passive patches cannot be installed in the case of 0.08.

3.3. Simulation of Attenuation Performance. The passive patch attenuation performance at the two selected positions is simulated by the loss factor and the reduced peak size. First, loss factors for each mode at two locations are compared. The loss factors at each location are given in Table 5.

Next, the frequency spectrum predicted from 0 to 1000 Hz at the observation point is shown. The observation point was selected as the normalization position of 0.375. Figure 10 shows the simulation of the accelerance from equation (29) for undamped beams and passive patches in two selected cases. The loss tends to be the same as the result of the loss factor, and it can be confirmed that the peak size is 0.82 at the resonance frequency except for mode 2. In addition, it is confirmed that a large attenuation is invoked in modes 3, 4, and 5 when a passive patch is attached at a position of 0.82. In the case of the natural frequency, it is confirmed that the stiffness and the mass of the system are changed by attaching the passive patch, and the natural frequency is decreased accordingly. That is, it can be seen that the effect of mass is greater than that of stiffness. The natural frequency does not drop much, but if the excitation at that frequency is large, the passive patch

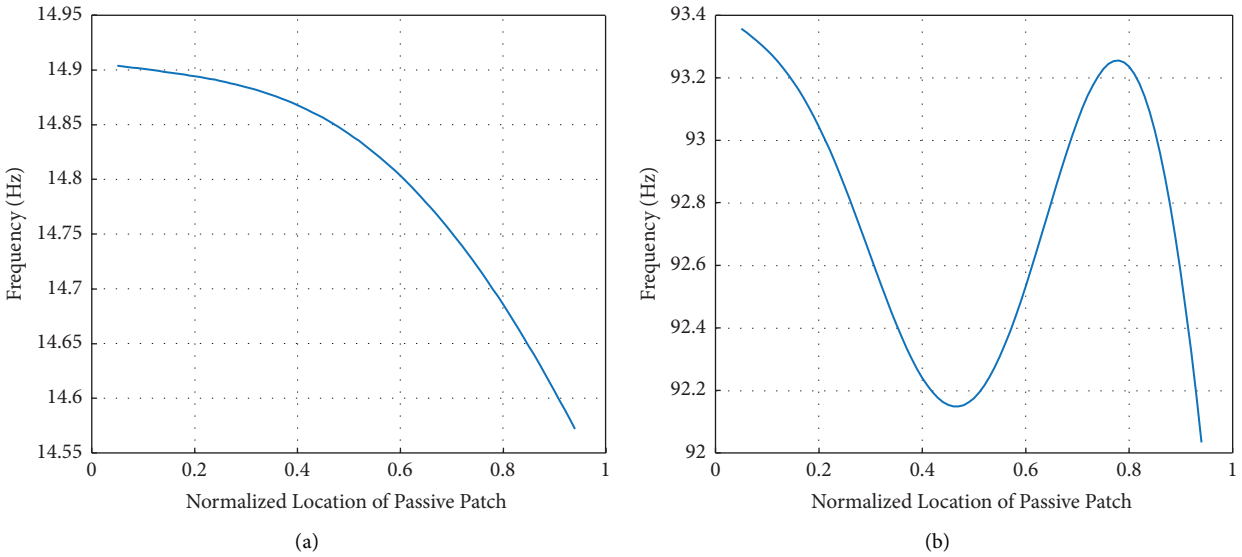

Figure 7: Natural frequency variation for the (a) 1st mode and (b) 2nd mode.

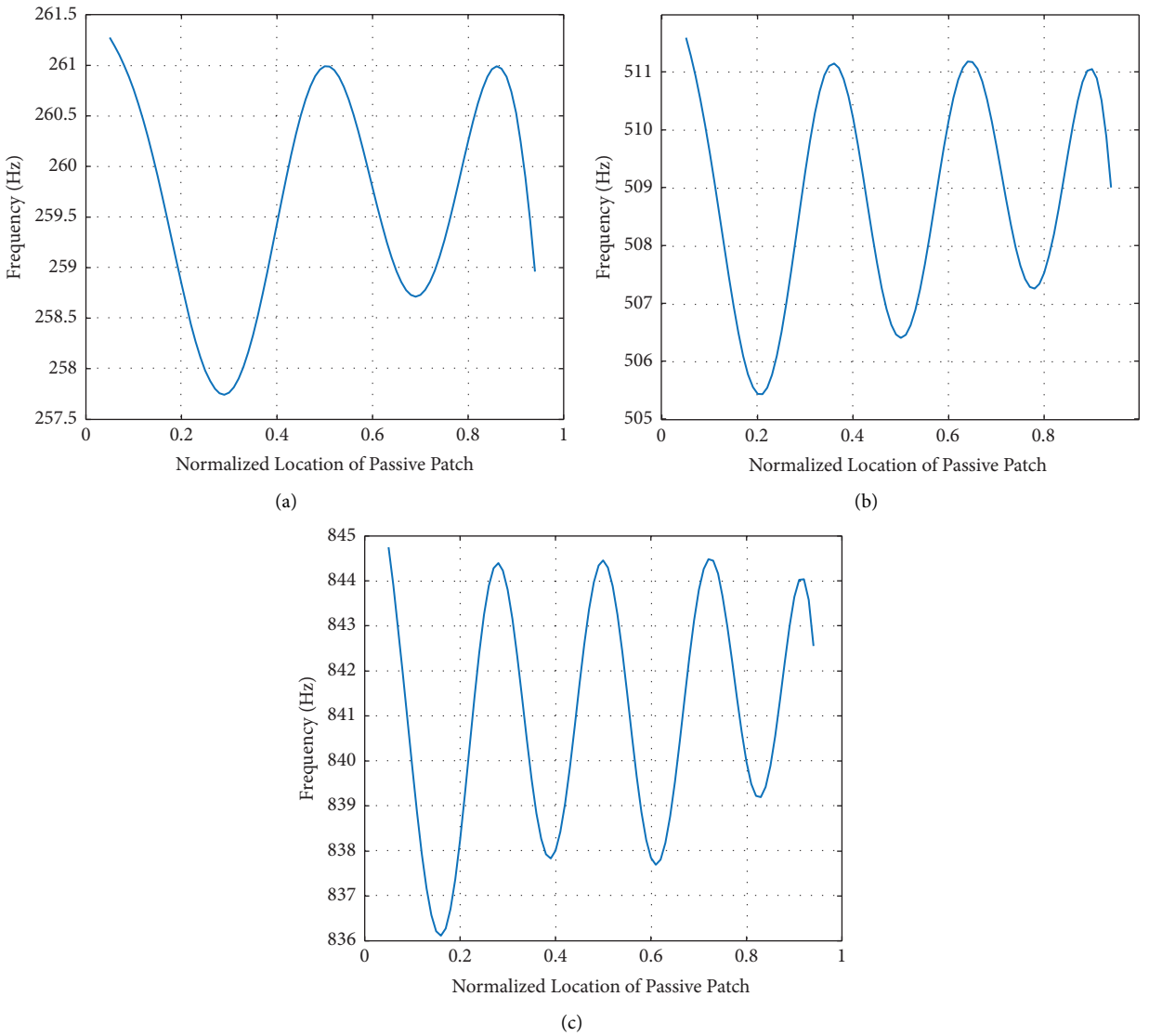

Figure 8: Natural frequency variation for the (a) 3rd mode, (b) 4th mode, and (c) 5th mode.

Table 3: Natural frequency change according to patch location.

Peak (Hz)	Mode 1	Mode 2	Mode 3	Mode 4	Mode 5
Without patch	15	93	261	512	848
Located in 0.5	15	91	260	504	838
Change	0.00%	−2.15%	−0.38%	−1.56%	−1.18%
Located in 0.82	15	93	260	507	839
Change	0.00%	0.00%	−0.38%	−0.98%	−1.06%

Table 4: Mode contributions for each mode.

	Mode 1	Mode 2	Mode 3	Mode 4	Mode 5
Mode contribution	0.02	0.12	0.30	0.53	0.78

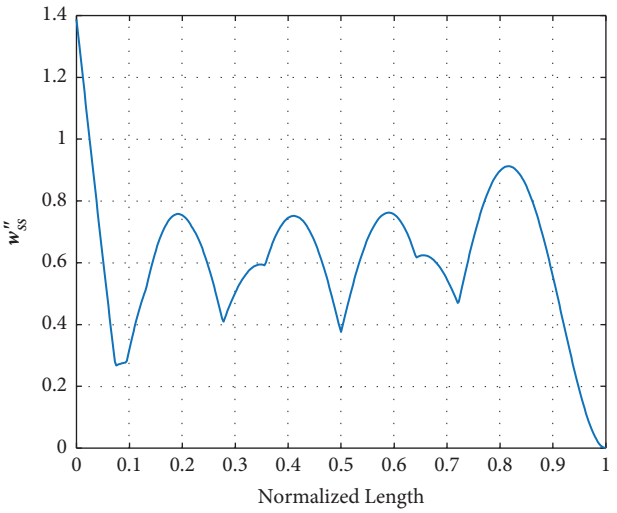

Figure 9: Calculated w_{ss}''.

Table 5: Loss factor for each mode.

Patch location	Mode 1	Mode 2	Mode 3	Mode 4	Mode 5
0.82	0.0002	0.0010	0.0028	0.0042	0.0032
0.5	0.0015	0.0025	0.0002	0.0030	0.0009

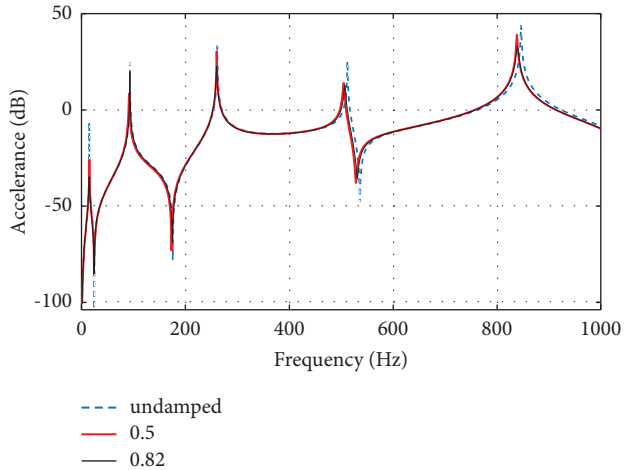

Figure 10: Accelerance of nonattenuated and attenuated beams (simulation).

should be avoided. The size of the reduced peak produced by attaching the passive patch is given in Table 6. The data written in the table indicates the decibel size before attachment and at position 2 and the reduction amount at the resonance frequency corresponding to each mode. Therefore, the frequencies at the compared peaks are all different.

In Table 6, the reduction of the peak is compared with the resonance frequency in one mode, and it is confirmed that attenuation is large when the loss coefficient is large, except for mode 1 (with the patch at 0.82). In Figure 10, it can be observed that mode 1 has relatively small amplitude compared to the other modes and the amplitude level in the time domain is not much affected to those modes. However, if one passive patch is compared with the other modes, the loss factor is not necessarily large and the peak decrease is not always large.

3.4. Experimental Validation. Next, the effect of the position of the passive patch in the two selected cases was verified by experiments. Figure 11 shows the experimental equipment. An accelerometer is mounted on a thin beam fixed to the vise, and an impact hammer is used to generate the impulse. The signal from the accelerometer is received from the data collector and displayed on the monitor through signal processing. The sampling frequency is 2000 Hz, observed from 0 Hz to 1000 Hz in total, and the frequency resolution is 0.1 Hz.

Figure 12 shows the position of the beam on the beam and the observation position of the response. In the case of excitation, it is assumed that a constant probability distribution is applied in the range of the normalization length of 0.1. Therefore, the excitation position is divided into three parts, and averaging is performed. Figure 13 shows the attached passive patch.

Figure 14 shows the acceleration measured by the accelerometer. In this case, it is possible to observe that a different peak appears from the simulation. This is because the length is longer than 10 times the width, but other modes such as twist have also appeared in the region above 250 Hz. If the same results with simulation need to be obtained through the experiment, the system should be modelled by a thin plate model. In addition, the clearly appeared modes besides bending modes are because of the contact condition of beam and vise, which is an incomplete supporting condition exciting other structures such as vise, vibration table, etc. The yellow circles indicate the bending mode, and it is confirmed that the first to fifth modes are displayed in order. As with the simulation, it is confirmed that the natural frequency of each mode is reduced by attaching the passive patch.

Also, Table 7 lists the peak magnitude at resonance frequency in decibels for each mode and the attenuation performance when attached at the normalization position of 0.5 compared to the normalization position of 0.8 for mode 1 and mode 2. However, for modes 3, 4, and 5, it is confirmed that the passive patch attached to 0.82 shows much better attenuation performance. As the mode contribution is large

Table 6: Peak-to-peak of each mode for manual patching in both cases.

Peak (dB)	Mode 1	Mode 2	Mode 3	Mode 4	Mode 5
W/o patch	−6.16	24.53	33.33	25.39	43.7
With 0.5	−25.87	8.394	30.5	14.01	39.09
Change	19.71↓	16.136↓	2.83↓	11.38↓	4.61↓
With 0.82	−34.69	20.12	22.7	12.82	33.2
Change	28.53↓	4.41↓	10.63↓	12.57↓	10.5↓

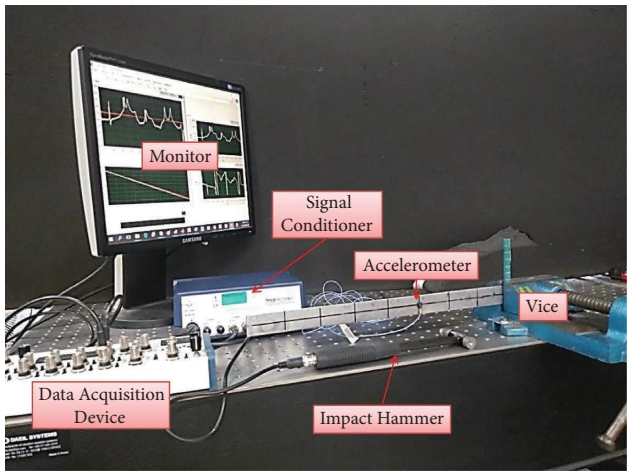

Figure 11: Experimental equipment configuration and labels.

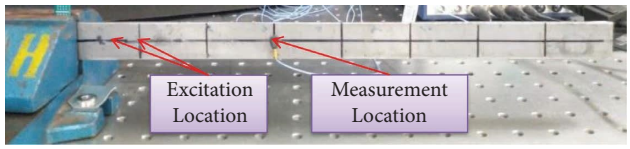

Figure 12: Excitation and measurement positions.

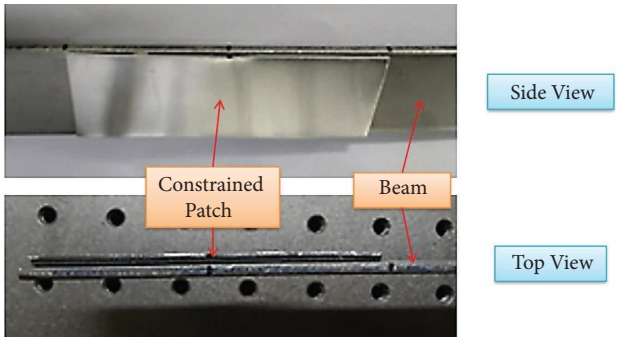

Figure 13: Attached passive patch.

in modes 3, 4, and 5, it is targeted mainly at the high modes, and the result is also the result of the experiment. In mode 4, it is confirmed that large attenuation occurs. This is because the resonance frequency of the twist mode near 500 Hz, which is the resonance frequency of mode 4, is reduced by about 30 Hz with the passive patch attachment.

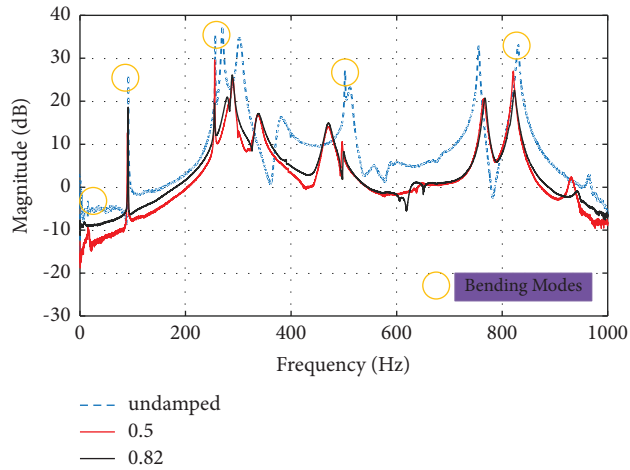

Figure 14: Frequency response function according to the position of passive patch.

Table 7: Peak-to-peak and size reduction for each mode for manual patching in both cases.

Peak (dB)	Mode 1	Mode 2	Mode 3	Mode 4	Mode 5
W/o patch	−2.72	26.15	35.52	27.21	30.67
With 0.5	−9.13	12.67	29.61	10.58	27.02
Change	6.41↓	13.48↓	5.91↓	16.63↓	6.23↓
With 0.82	−9.02	18.64	19.52	8.26	22.51
Change	6.3↓	7.51↓	16↓	18.95↓	10.74↓

Figure 15 compares the peak-to-peak values obtained through experiments and simulations. For the positions of each passive patch, the experiment and the simulation are similar in the remaining areas except for mode 1 and there is a larger decrease in the value of the peak in the experiment. This is presumably because the passive patch reduces not only the bending mode but also the other modes. Further, in mode 1, the attenuation in the simulation was large. In the experiment, the resonance frequency of mode 1, which is a small signal, is not well represented by the noise. Figure 16 shows the correlation between the loss factor and attenuation levels in dB scale obtained from simulation and experiment, which obviously shows the same trend except for mode 1 from the simulation.

Figure 17 shows the frequency spectrum on a linear scale. This metric can be used to determine the RMS value for measuring the overall vibration attenuation, and its value is given in Table 8. Comparing the case where the passive patch is not attached and the case where the passive patch is attached at 0.5 position, it is confirmed that the vibration of about 27% is totally reduced.

In addition, it is confirmed that the size of the RMS is further reduced to 41.9% when it is attached to the normalization position 0.82. Amplitude attenuation occurs not only in bending but in other modes as well. When the peak and RMS size are reduced, the design of the passive patch is considered appropriate.

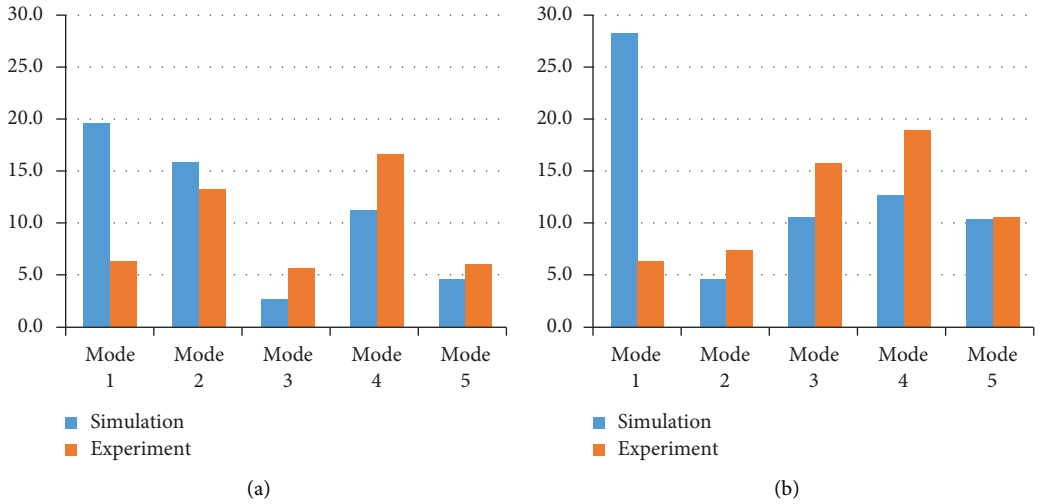

Figure 15: Comparison of peak-to-peak attenuation in the dB scale (simulation vs. experiment) corresponding to the patch location of (a) 0.5 mm and (b) 0.82 mm.

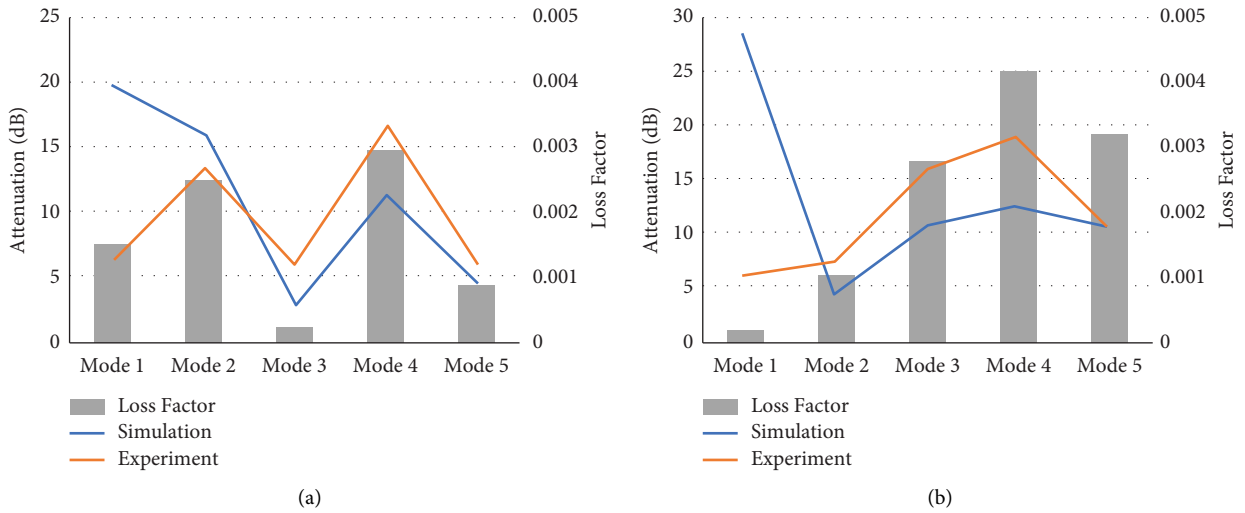

Figure 16: Correlation analysis with patch at (a) 0.5 and (b) 0.82.

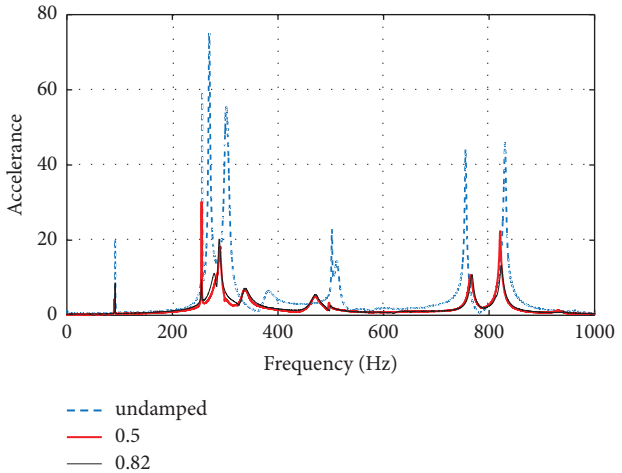

Figure 17: The frequency spectrum according to the position of the passive patch (linear scale).

Table 8: RMS reduction for manual patching in both cases.

RMS	Total
Before attachment	9.62
With 0.5	7.04
Change	2.58 (26.8%↓)
With 0.82	5.59
Change	4.03 (41.9%↓)

4. Conclusion

To optimize the position of the passive patch, the sum of squares of the bend shape and the position of the passive patch are used. Further, the effect of the passive patch is verified by using the existing passive patch model.

First, the model expression of the passive patch is examined. The relationship between the passive patch and the beam is investigated in detail, and the loss coefficient and the frequency spectrum due to the natural frequency and the forced vibration in the presence of several passive patches are numerically simulated.

Next, in order to determine the position of the passive patch, the change in the loss coefficient and natural frequency according to the position is examined. It is confirmed that the loss factor is dependent on the curvature which is the second derivative of the bending mode shape. The position of the passive patch is determined through the sum of squares value expressed as a linear combination of mode shape and mode contribution. Passive patches of constant length and thickness are designed in this way. Weighting is applied to the case where the mode contribution is large so that the attenuation effect is enhanced in a mode in which a large response is expected. It is confirmed that the natural frequency is lowered for each mode due to the passive patch changing the vibration system.

In order to verify the performance of the positionally determined passive patch, two cases are compared. It is assumed that one passive patch is designed to have a constant length on one cantilevered beam. In this case, the passive patch attenuates the overall vibration, and the peak-to-peak value also decreases regardless of position. However, it can be seen that the size of the response is greatly reduced in the case of the passive patch, determined by obtaining the sum of squares using the shape function. Experiments were conducted to verify the effectiveness of passive patches. Experimental results show that the frequency response in mode 1 is small and difficult to observe. Because the experiment involves a three-dimensional mode of vibration, other peaks also appear, which is different from the simulation. The attenuation effect on the bending of the passive patch was not accurately observed, while the natural frequency was shifted by the passive mode such as the twist mode.

Future research should investigate applying the passive patch design method to the actual vibration system by the excitation force of various frequency spectrums. In this study, a certain size is assumed and used to verify the damping effect using the proposed method considering the mode shape and frequency of the actual model.

In addition, it is necessary to study the optimization method of the position design in installing passive patches as well as active patches using the piezoelectric element. Passive patches are effective at high frequencies, so weights can be applied to achieve optimal vibration damping along with active patches.

The passive patch location design method proposed in this paper is expected to contribute to the improvement of the practical application of passive patches without the need for complicated processes. In addition, if applied to real machine systems with active control, this method will contribute to the research corpus on the topic of next generation vibration reduction systems.

Data Availability

The data presented in this study are available on request from the corresponding author.

Conflicts of Interest

The authors declare that they have no conflicts of interest.

Acknowledgments

This work was supported by the 2023 Yeungnam University Research Grant (223A380081) and by Basic Science Research Program through the National Research Foundation of Korea (NRF) funded by the Ministry of Education (NRF-2022R1F1A1076089).

References

[1] M. D. Rao, "Recent applications of viscoelastic damping for noise control in automobiles and commercial airplanes," *Journal of Sound and Vibration*, vol. 262, no. 3, pp. 457–474, 2003.

[2] B. Baran, Y. Yesilce, and S. Catal, "Free vibrations of axial-loaded beams resting on viscoelastic foundation using Adomian decomposition method and differential transformation," *Engineering Science and Technology, an International Journal*, vol. 73, no. 2, pp. 109–121, 2020.

[3] B. Bozyigit, Y. Yesilce, and M. Abdel Wahab, "Single variable shear deformation theory for free vibration and harmonic response of frames on flexible foundation," *Engineering Structures*, vol. 208, Article ID 110268, 2020.

[4] B. Baran, Y. Yesilce, and M. Abdel Wahab, "Transfer matrix formulations and single variable shear deformation theory for crack detection in beam-like structures," *Structural Engineering and Mechanics*, vol. 73, no. 2, pp. 109–121, 2020.

[5] B. Baran, Y. Yesilce, and M. Abdel Wahab, "Free vibration and harmonic response of cracked frames using a single variable shear deformation theory," *Structural Engineering and Mechanics*, vol. 74, no. 1, pp. 33–54, 2020.

[6] L. Irazu and M. J. Elejabarrieta, "The influence of viscoelastic film thickness on the dynamic characteristics of thin sandwich structures," *Composite Structures*, vol. 134, pp. 421–428, 2015.

[7] A. Benjeddou, "Advances in hybrid active-passive vibration and noise control via piezoelectric and viscoelastic constrained layer treatments," *Journal of Vibration and Control*, vol. 7, no. 4, pp. 565–602, 2001.

[8] M. A. Trindade and A. Benjeddou, "Hybrid active-passive damping treatments using viscoelastic and piezoelectric materials: review and assessment," *Journal of Vibration and Control*, vol. 8, no. 6, pp. 699–745, 2002.

[9] A. K. Lall, N. T. Asnani, and B. C. Nakra, "Damping analysis of partially covered sandwich beams," *Journal of Sound and Vibration*, vol. 123, no. 2, pp. 247–259, 1988.

[10] A. K. Lall, N. T. Asnani, and B. C. Nakra, "Vibration and damping analysis of rectangular plate with partially covered con-strained viscoelastic layer," *Journal of Vibration and Acoustics*, vol. 109, no. 3, pp. 241–247, 1987.

[11] S. W. Kung and R. Singh, "Vibration analysis of beams with multiple constrained layer damping patches," *Journal of Sound and Vibration*, vol. 212, no. 5, pp. 781–805, 1998.

[12] S. W. Kung and R. Singh, "Complex eigensolutions of rectangular plates with damping patches," *Journal of Sound and Vibration*, vol. 216, no. 1, pp. 1–28, 1998.

[13] S. W. Kung and R. Singh, "Development of approximate methods for the analysis of patch damping design concepts," *Journal of Sound and Vibration*, vol. 219, no. 5, pp. 785–812, 1999.

[14] J. Plattenburg, J. T. Dreyer, and R. Singh, "Active and passive damping patches on a thin rectangular plate: a refined analytical model with experimental validation," *Journal of Sound and Vibration*, vol. 353, no. 29, pp. 75–95, 2015.

[15] S. Tian, Z. Xu, Q. Wu, and C. Qin, "Dimensionless analysis of segmented constrained layer damping treatments with modal strain energy method," *Shock and Vibration*, vol. 2016, Article ID 8969062, 16 pages, 2016.

[16] B. Khalfi and A. Ross, "Influence of partial constrained layer damping on the bending wave propagation in an impacted viscoelastic sandwich," *International Journal of Solids and Structures*, vol. 50, no. 25-26, pp. 4133–4144, 2013.

[17] H. Zheng, C. Cai, and X. M. Tan, "Optimization of partial constrained layer damping treatment for vibrational energy minimization of vibrating beams," *Computers and Structures*, vol. 82, no. 29-30, pp. 2493–2507, 2004.

[18] H. Zheng, C. Cai, G. S. H. Pau, and G. R. Liu, "Minimizing vibration response of cylindrical shells through layout optimization of passive constrained layer damping treatments," *Journal of Sound and Vibration*, vol. 279, no. 3-5, pp. 739–756, 2005.

[19] Y. Lei, W. Zheng, Q. Huang, and C. Li, "Topology optimization of passive constrained layer damping on plates with respect to noise control," *Advanced Materials Research*, vol. 774-776, pp. 3–6, 2013.

[20] W. Zheng, Y. Lei, S. Li, and Q. Huang, "Topology optimization of passive constrained layer damping with partial coverage on plate," *Shock and Vibration*, vol. 20, no. 2, pp. 199–211, 2013.

[21] Z. Fang, "Topology optimization approach of constrained layer damping layout using level set method," *International Congress on Sound and Vibration*, vol. 18, 2014.

[22] A. L. Araújo, P. Martins, C. M. Mota Soares, C. A. Mota Soares, and J. Herskovits, "Damping optimization of viscoelastic laminated sandwich composite structures," *Structural and Multidisciplinary Optimization*, vol. 39, no. 6, pp. 569–579, 2009.

[23] A. El Hafidi, C. D. L. P. Herrero, and B. Martin, "Optimization of passive constrained layer damping (PCLD) treatments for vibration reduction," *Journal of Vibroengineering*, vol. 17, no. 6, pp. 3035–3045, 2015.

[24] E. Askar, E. Elsoaly, M. Kamel, and H. Kamel, "Optimization of passive vibration damping of space structures," *International journal of mechanical, aerospace, industrial, mechatronic and manufacturing engineering*, vol. 11, 2017.

[25] E. M. Kerwin and Kerwin Jr., "Damping of flexural waves by a constrained viscoelastic layer," *Journal of the Acoustical Society of America*, vol. 31, no. 7, pp. 952–962, 1959.